applied sciences

MDPI

Article

Experimental Study on Pore Structure Evolution of Unloaded Rock Mass during Excavation of Reservoir Slope under Dry–Wet Cycle

Lili Chen, Xingzhou Chen *, Sheng Gong, Zhenhan Li and Zhenkun Su

School of Architecture and Civil Engineering, Xi'an University of Science and Technology, Xi'an 710054, China; chenllchen@163.com (L.C.); shenggong1123@163.com (S.G.); zhli0605@163.com (Z.L.); zksu1022@163.com (Z.S.)
* Correspondence: xzchen0416@xust.edu.cn

Abstract: There is a long sequence of periodic characteristics of reservoir water storage and discharge in large hydropower stations. The unloaded rock mass formed by blasting and excavation in the reservoir slope of the reservoir fluctuation zone is not only subjected to the penetration erosion caused by the change of the water level of the reservoir slope, but also the dry–wet cycle caused by the reservoir water storage and discharge. There is an obvious process of crack derivation and pore structure expansion, and the subsequent strength degradation breeds reservoir slope risks, which is one of the important factors restricting the operation safety of power stations. To study the pore structure evolution law of unloaded rock mass in reservoir slope excavation of reservoir fluctuation zones, the dry–wet cycle test simulating the periodic storage and discharge environment was carried out with samples of equal unloading amount obtained by indoor triaxial unloading test. The variation law of mesoscopic parameters such as wave velocity, mass, and nuclear magnetic resonance spectrum under dry–wet cycle was compared and analyzed, and the physical and mechanical mechanism of the pore structure evolution of the unloaded specimen under dry–wet cycles was explored. The results show that: (1) With the increase of dry–wet cycles, the evolution of wave velocity and dry mass of unloaded samples has obvious stage characteristics, which generally presents a rapid change in the early stage, moderate in the middle stage, and gradually stable in the late stage; (2) nuclear magnetic resonance (NMR) shows that the number of macropore structures in unloaded samples increases gradually with the dry–wet cycles; (3) the smaller the initial confining pressure, the larger the first peak area and the peak value of unloaded samples, and the spectral area corresponding to each peak under low confining pressure is significantly larger than that under medium and high confining pressure; (4) the unloading amount affects the overall proportion of macropores in the sample, which determines the deterioration process and evolution law of the mesostructure of the sample under dry–wet cycles.

Keywords: slope and fluctuation zone; excavation and unloading; dry–wet cycle; NMR analysis

Citation: Chen, L.; Chen, X.; Gong, S.; Li, Z.; Su, Z. Experimental Study on Pore Structure Evolution of Unloaded Rock Mass during Excavation of Reservoir Slope under Dry–Wet Cycle. *Appl. Sci.* **2024**, *14*, 4716. https://doi.org/10.3390/app14114716

Academic Editor: Tiago Miranda

Received: 9 May 2024
Revised: 27 May 2024
Accepted: 27 May 2024
Published: 30 May 2024

1. Introduction

In addition to the Three Gorges Project, the reservoir area of large-scale hydropower projects in China often has a narrow and deep canyon field environment. The typical characteristics of high dams and large reservoirs and the large-scale water level drop caused by flood discharge can easily induce hydraulic erosion, seepage, latent erosion, dry–wet cycles, and other thorny problems in the reservoir fluctuation area that affect the stability of unloading rock mass after excavation of reservoir slopes [1]. On the one hand, the compound environment formed by high dams, large reservoirs, and narrow deep canyons provides a prerequisite for the excavation unloading rock mass in the water-fluctuation zone to fully soak and withstand high seepage pressure during the gradual impoundment of the reservoir. On the other hand, due to the comprehensive consideration of the maintenance of power stations, flood control of the reservoir and the prevention

of infiltration damage of the slope, the large-scale sudden drop of water level forces the excavated reservoir slope of reservoir water-fluctuation zone to bear a sharp dry–wet cycle, which aggravates the structural deterioration of unloaded rock mass. Generally speaking, the open pores and cracks of the excavation unloading rock mass of the reservoir slope can be saturated under the impoundment, but the reservoir water drainage process cannot achieve its complete drainage. Under the induction of sunlight on the slope surface and the thermal conductivity of the rock mass, the deterioration of the pore structure of the rock mass induced by dry–wet cycle is bound to be more prominent in the reservoir slope of the reservoir fluctuation zone. Furthermore, the study of the dry–wet cycle of unloaded rock mass in reservoir slopes is of practical significance for comprehensively exploring the macro-meso-structure evolution mechanism of excavated rock mass on reservoir slopes in water-fluctuation zones.

Excavation unloading exists widely in various kinds of geotechnical engineering construction; Ha and Li [2] first began to study unloading rock mass mechanics in China, then many scholars at home and abroad also conducted in-depth research on unloading rock mass mechanics. Most of them start from the triaxial unloading test to study the crack evolution and failure mechanism, mechanical parameter damage degradation effect, and strength characteristics of various rocks during unloading [3–6]. Considering the influence of unloading rate on rock failure mode, triaxial unloading tests under different unloading rates were designed and carried out to analyze the failure characteristics of rock [7–10]. On this basis, many scholars intervened in the influence of various unloading paths and studied the energy evolution characteristics of rock in triaxial unloading failure processes from macro and meso perspectives [11–13].

With the gradual enrichment of test methods, many achievements have been made on the influence of dry–wet cycles on rocks from a microscopic point of view. Zhang et al. [14] and Guo et al. [15] established the relationship between structural characteristics, fracture development trend, fractal dimension, and correlation dimension by analyzing the crack growth and acoustic emission characteristics of samples and studied the water weakening effect of dry–wet cycling on rocks. Based on the scanning electron microscope (SEM) test, Wang et al. [16] proposed the concept of erosion degree of argillaceous sandstone under dry–wet cycles based on the analysis of mesoscopic images of rock samples with different dry–wet cycles and established the relationship between mesoscopic and macroscopic. On this basis, Chen et al. [17] and Qin et al. [18] established the meso-damage evolution equation based on fractal dimensions and studied the influence of dry–wet cycles on meso-characteristics of altered granite. Some scholars have also studied the effect of cyclic dry–wet conditions on sandstone by visualizing and quantifying the distribution of microstructure in rock through 3D reconstruction and mixed image segmentation of CT images [19,20] and surface topography scanning tests [21]. Dang et al. [22] analyzed the relationship between pore size changes and porosity through NMR tests and studied the evolution of microscopic pore structure of rocks and soils after different dry–wet cycles.

Many scholars have studied the damage characteristics of rocks caused by dry–wet cycle by various monitoring methods. Fu et al. [23] comprehensively carried out uniaxial compression tests, splitting tests, and full-section CT scanning tests to analyze the meso-damage evolution law of sandstone. Liu et al. [24] discussed the strength degradation and microstructure changes of sandstone under dry–wet cycles through uniaxial compression, triaxial compression and scanning electron microscopy tests. Wen et al. [25], Huang et al. [26], and Wang et al. [27] studied the microstructural changes of sandstone under dry–wet cycles by uniaxial compressive strength test, SEM, and backscattered electron image (BSE). Yang et al. [28], Ma et al. [29], and Zhao et al. [30] comprehensively used SEM, NMR, CT cross section scanning, and 3D reconstruction experiments to analyze the microstructure evolution of sandstone under dry–wet cycles and revealed the deterioration characteristics and mechanism of rock mass in the fluctuating zone of the Three Gorges reservoir area.

Based on mechanical tests and microscopic monitoring methods, the above studies studied the failure mechanism during unloading and the influence of dry–wet cycles on the microscopic structure of rock. At the same time, under the action of excavation unloading, the deterioration characteristics of rock mass will directly affect the deformation and stability of reservoir slopes. It is necessary to study the deterioration mechanism of excavated slopes under water–rock interaction [31]. Therefore, based on the above research results, this paper superimposes and considers the occurrence environment characteristics of the reservoir slope undergoing excavation unloading and long-term periodic storage and discharge in the reservoir area, takes the unloaded samples of different degrees obtained from the staged unloading test as the research object, and adopts the rapid cycle of "drying-saturation-drying" in the laboratory to approximately simulate the long-term repeated fluctuation of the water level in the reservoir area. By means of NMR, the pore evolution characteristics of rocks under dry–wet cycles are analyzed from a mesoscopic perspective. The research results can provide theoretical reference for the structural deterioration and deformation control of rock mass on reservoir slopes.

2. Test Overview

2.1. Sample Preparation

The rock blocks collected from the reservoir slope of a power station reservoir were taken as the objects and were processed into 50 mm × 100 mm standard samples according to the requirements of the "Standard for test methods of engineering rock mass" [32], and the error was ±0.5 mm. The mean value of basic physical parameters of each sample is shown in Table 1, and the wave velocity dispersion diagram of each sample is shown in Figure 1, which shows that the dispersion of the sample is small.

Table 1. Mean values of physical parameters of samples.

Diameter/mm	Height/mm	Mass/g	Density/(g/cm^3)	Wave Velocity/(km/s)	Porosity
49.84	100.15	457.16	2.36	2.83	9.49%

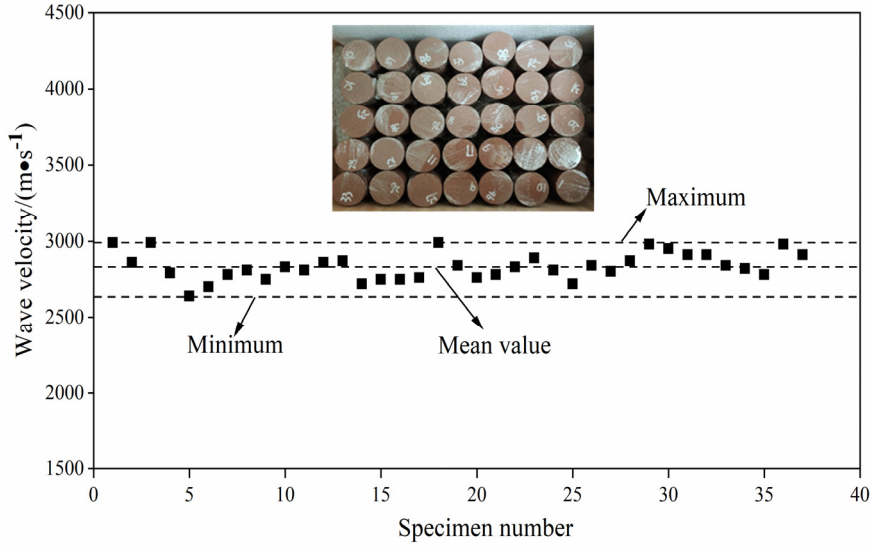

Figure 1. Wave velocity distribution of samples.

2.2. Preparation of Unloaded Samples

In view of the fact that the stress release of original rock induced by partial excavation in engineering leads to the phenomenon of different unloading amounts, and the confining pressure unloading is more suitable for the stress environment after stress disturbance in the engineering site, the effects of unloading amount and unloading rate were comprehensively

considered in the unloaded samples preparation test, and Equation (1) was used as the division standard to define the unloading amount of confining pressure to characterize the damage degree of unloaded samples [33].

$$U_S = \frac{\left(\sigma_3^0 - \sigma_3^i\right)}{\left(\sigma_3^0 - \sigma_3^f\right)} \times 100\% \quad (1)$$

where U_S is the confining pressure unloading amount, σ_3^0 is the confining pressure value before unloading, σ_3^i is the confining pressure value when unloading to level i, and σ_3^f is the confining pressure value when triaxial unloading failure occurs.

According to the test design, a graded unloading test under the proposed confining pressure and unloading amount is carried out to obtain the unloaded samples. The stress path is shown in Figure 2. The test details of the installation of the specimen are shown in Figure 3. Stage OA is the hydrostatic pressure stage, which adds axial pressure and confining pressure at the same rate to the initial confining pressure setting value. In stage AB, confining pressure is kept constant, and axial pressure is added to 70% of the peak value of triaxial strength under a specific confining pressure [34]. Stage BC is the constant axial compression stage, keeping axial pressure constant and unloading confining pressure in stages. Stage CD is the axial pressure unloading stage, keeping confining pressure unchanged and unloading axial pressure to the magnitude of confining pressure. Stage DO is the stage of unloading the remaining axial pressure and confining pressure at the same rate.

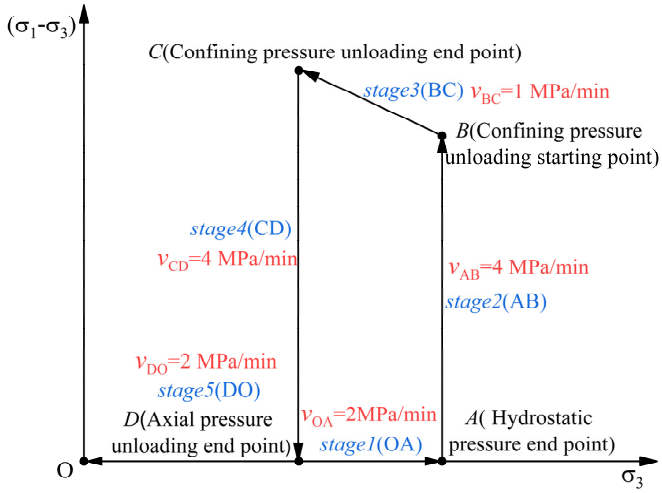

Figure 2. Stress path of unloaded sample preparation test flow.

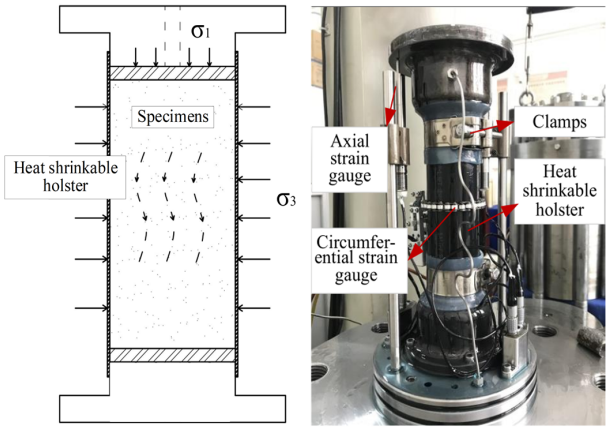

Figure 3. Test details of mounting specimens.

2.3. Test Flow

The specific test flow is shown in Figure 4.

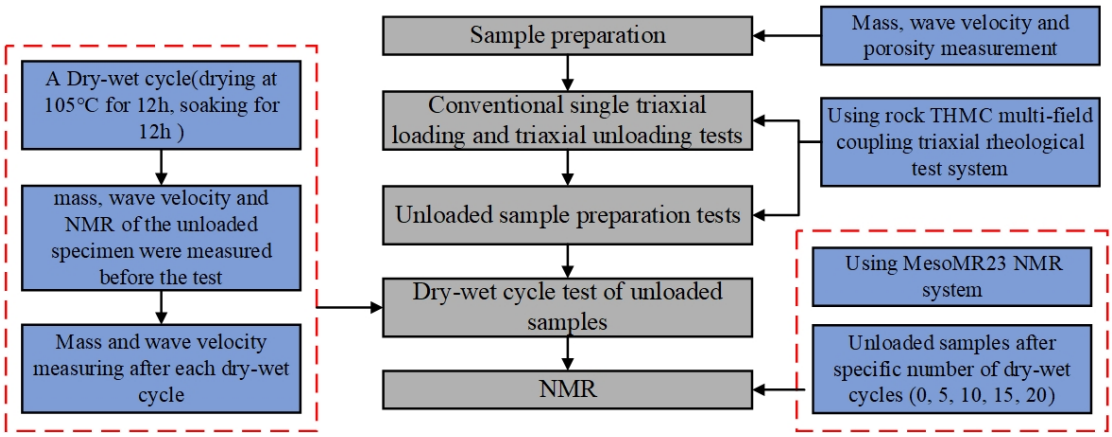

Figure 4. Test flow chart.

(1) Laboratory mechanical test

Considering the established stress environment of slope rock mass with excavation disturbance, in situ stress of 18 MPa obtained from borehole data in the field is taken as the upper limit of lateral stress and as the boundary condition for simulating lateral stress of slope.

Based on the above considerations, the saturated sandstone samples were subjected to triaxial compression tests with confining pressures of 0, 9, 12, and 15 MPa and triaxial unloading tests with corresponding confining pressures, respectively. The maximum axial pressure of the triaxial unloading test was 70% of the peak strength of the sample under the corresponding confining pressure [35], and the triaxial loading and unloading test results of the samples were obtained as shown in Table 2. The formula in brackets represents the calculation process of 70% of the triaxial peak strength under corresponding confining pressure, and it is used as a reference for unloading amount.

Table 2. Results of laboratory conventional mechanical tests.

Test Types	Maximum Axial Pressure/(MPa)	Confining Pressure during Unloading Failure/(MPa)
Uniaxial Compression Test	48	——
Triaxial Compression Test (Confining pressure 9 MPa)	115	——
Triaxial Compression Test (Confining pressure 12 MPa)	127	——
Triaxial Compression Test (Confining pressure 15 MPa)	140	——
Triaxial Unloading Test (Confining pressure 9 MPa)	81 (115 × 0.7)	2.5
Triaxial Unloading Test (Confining pressure 12 MPa)	89 (127 × 0.7)	4
Triaxial Unloading Test (Confining pressure 15 MPa)	98 (140 × 0.7)	5.4

(2) Preparation of unloaded samples

Based on the results of conventional triaxial loading and unloading tests in the laboratory, three confining pressures of 9, 12, and 15 MPa with the magnitude of 80% unloading [33] were selected, and the stress–strain curves of the proposed confining pressure of the unloaded samples were obtained as shown in Figure 5, and the corresponding stages were referred to in Figure 2.

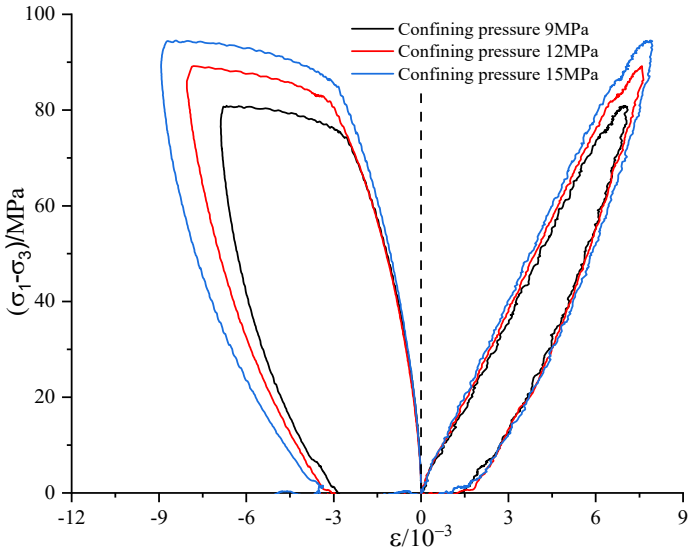

Figure 5. Unloading stress–strain curve at 80% unloading amount.

It can be seen from Figure 5 that there is a large overlap of hysteresis loops under different upper limit stress conditions, which depends on the initial confining pressure and is mainly reflected in stage 2. With the increase of initial confining pressure, the area of the hysteresis loop increases gradually, and the corresponding area increase ratio shows an accelerating trend. Compared with the lateral strain, the axial strain changes relatively evenly and approximately linearly in each stage. The lateral strain expansion includes linear and nonlinear stages. In unloading stages, the strains are quite different and show a significant nonlinear trend. Compared with stage 1, the lateral strain variation of stage 5 decreases significantly, and the maximum is only about 40% of stage 1. The main reason is that during the process of confining pressure grading unloading, the activity of microcracks increases rapidly, the volume of the sample increases, and part of the deformation caused is irrecoverable. It is reflected from the side that the confining pressure unloading stage is the main stage of the load-induced damage of the sample.

(3) Dry–wet cycle test

Taking the number of dry–wet cycles as the grouping standard, the unloaded samples were divided into five groups. The test was set to dry in the oven at 105 °C for 12 h and fill with water for 12 h as a dry–wet cycle. The mass and wave velocity of each sample after each dry–wet cycle were measured, respectively, and the variation of mass and wave velocity of unloaded samples with dry–wet cycles was analyzed.

(4) NMR

An NMR spectrometer (MesoMR23-060H-I) was used to carry out the test. The pore size distribution was determined by analyzing the relaxation characteristics of hydrogen-containing fluids (such as water) in rock pores. And the T2 spectrum area was obtained by integrating the signal intensity under the T2 spectrum. NMR tests were carried out on unloaded samples subjected to specific dry–wet cycles (0, 5, 10, 15, 20). The T_2 spectrum and spectral area parameters of the pore structure of the samples under different dry–wet cycles were obtained, and the macro and micro structure evolution characteristics of the samples under the superposition of unloading and dry–wet cycles were studied by combining the mass and wave velocity changes of the samples.

3. Wave Velocity and Mass Variation of Unloaded Samples under Dry–Wet Cycle

3.1. P-Wave Velocity

We use NM-4B non-metallic ultrasonic testing analyzer and ultrasonic pulse technology to calculate the P-wave velocity of rocks according to the ratio of the length of the

sample to the round-trip time of the ultrasonic wave through the sample. The velocity of P-wave can reflect the existence state of internal structure and crack to a certain extent. If there are micro-cracks or weak planes in rock, the propagation speed of the ultrasonic wave will be greatly reduced, and the reduction degree of sound speed is closely related to the number, compactness, and continuity degree of cracks. Figure 6 shows the variation curve of the P-wave velocity with cycles under the dry state of unloaded samples with different initial confining pressures at 80% unloading amount.

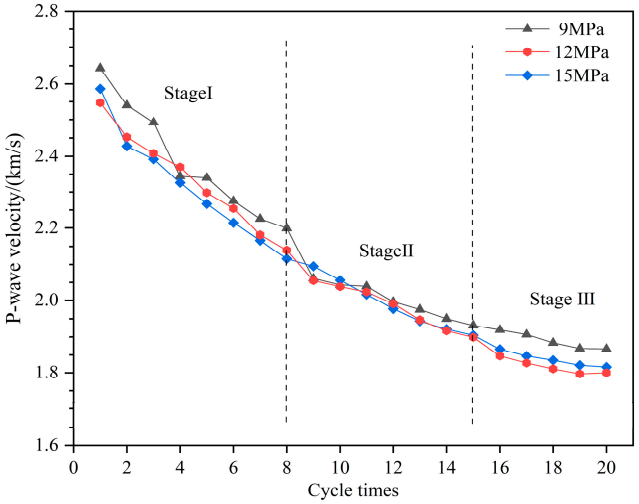

Figure 6. Variation curves of mean wave velocity of unloaded samples with cycles.

It can be seen from Figure 6 that the variation trend of wave velocity of unloaded samples with dry–wet cycle in the selected unloading amount and three confining pressure ranges shows three stages of rapid decrease-slow decrease-stability. In stage I (the first eight cycles), the wave velocity decreases non-linearly, the sample with initial confining pressure of 9 MPa has the largest wave velocity variation, and the cumulative reduction percentage is 60.94%. The wave velocity variation range of the sample with initial confining pressure of 12 MPa and 15 MPa is similar; the overall trend is that the larger dry–wet cycles, the smaller the reduction percentage. In stage II (8–15 cycles), the wave velocity changes more slowly than that of stage I, and the cumulative average reduction percentage is 31.36%. In stage II, the maximum reduction percentage was 12.14% for the sample with initial confining pressure of 9 MPa, and the minimum was 9.97% for the sample with initial confining pressure of 15 MPa. In stage III (15–20 cycles), the wave velocity of each sample is basically maintained at a steady state.

It can be seen that the damage of unloaded samples caused by the dry–wet cycle is a cumulative process. On the one hand, the damage crack caused by early unloading provides more crack channels for the dry–wet cycle, thus water easily infiltrates along the crack channels, which increases the pore water pressure, inter-cambium expansion, and inter-particle expansion and increases the crack. At the same time, water molecules slowly infiltrate into the sample along the cracks, causing the dissolution of soluble minerals and cements and causing the closed pores formed by the presence of cements to gradually transform into open pores. In stage I, the high content and solubility of soluble cement leads to continuous expansion and penetration of microcracks, and the number and volume of cracks increases rapidly. As the dry–wet cycle continues, various dissolved substances of the sample are transported and precipitated. In stage III, the content of soluble substances in the sample decreases, which leads to the weakening of the crack enlargement effect caused by the dissolution of cements, thus showing that the wave velocity changes tend to be stable.

3.2. Mass

The water absorption and dehydration characteristics of rocks are closely related to the pore characteristics. In the process of repeated water absorption and dehydration, the mass change can well reflect the progressive deterioration effect of the dry–wet cycle on unloaded rocks. Since the mass change is too small relative to the mass base of the sample, and the mass in the wet state has a large error in the measurement process, the mass in the dry state is used in this analysis. The variation curves of the sample with cycles under different confining pressures and unloading amount are drawn, as shown in Figure 7.

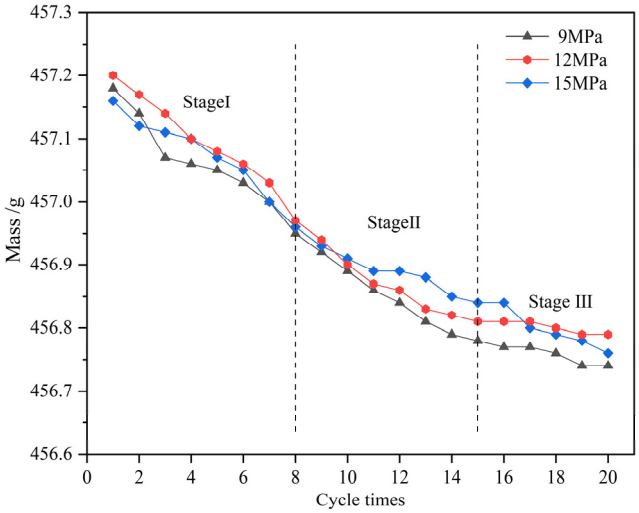

Figure 7. Variation curves of the mean mass of unloaded samples with cycles.

It can be seen from Figure 7 that the variation trend of unloaded sandstone after the dry–wet cycle can be roughly divided into three stages with the increase of cycles, which are rapid decrease, slow decrease, and steady state. In stage I (the first eight cycles), the mass decreased rapidly, the mass of each sample decreased by 0.22 g on average, and the cumulative average reduction percentage accounted for 52.79% of that of all stages. In stage II (8–15 cycles), the mass of the samples is in a relatively slow decreasing trend, and the total change of the stage is less than that of stage I. The mass of each sample is reduced by 0.15 g on average, and the cumulative reduction percentage accounted for 36.00% of all stages. In stage III (15–20 cycles), all the samples changed in the range of 0.08 g, and the mass change was relatively stable.

The mass of the sample decreases with the increase of cycles as a whole. On the one hand, the effect of water–rock interaction is manifested in the contact between particles and skeleton. The unloading effect first causes cracks to increase, and fine cracks appear at the contact of particles, which provides action channels for the later dry–wet cycle. That is, the pore of the sample continues to increase during the whole dry–wet cycle of the test, which is consistent with the wave velocity results. On the other hand, under the repeated lubrication and softening of water, mineral particles and soluble cements fall off, resulting in mass reduction [36]. There is little difference between the mass reduction rate of stage I and stage II, mainly because soluble substances and cements are dissolved and transported in water and are accumulate in closed pores in a short time without complete precipitation, resulting in a less significant dry–wet cycle effect of samples in stage I compared with stage II.

4. Pore Evolution Characteristics of Unloaded Samples under Dry–Wet Cycle

4.1. T_2 Spectrum Distribution

According to the basic theory of NMR, the relaxation time is consistent with the distribution of rock pore size. The smaller the transverse relaxation time, the smaller the pores. Jin et al. [37] divided the pores into micropores (T_2 < 10 ms), mesopores (10 ms < T_2 < 100 ms)

and macropores (T_2 > 100 ms) according to T_2 value. To analyze the pore evolution law of unloaded samples under different initial confining pressure at 80% unloading amount, the T_2 spectrum distribution of samples under different dry–wet cycles is plotted, as shown in Figure 8, and the variation curves of different pore proportions with dry–wet cycles are shown in Figure 9. (Note: n represents the number of cycles in the legend).

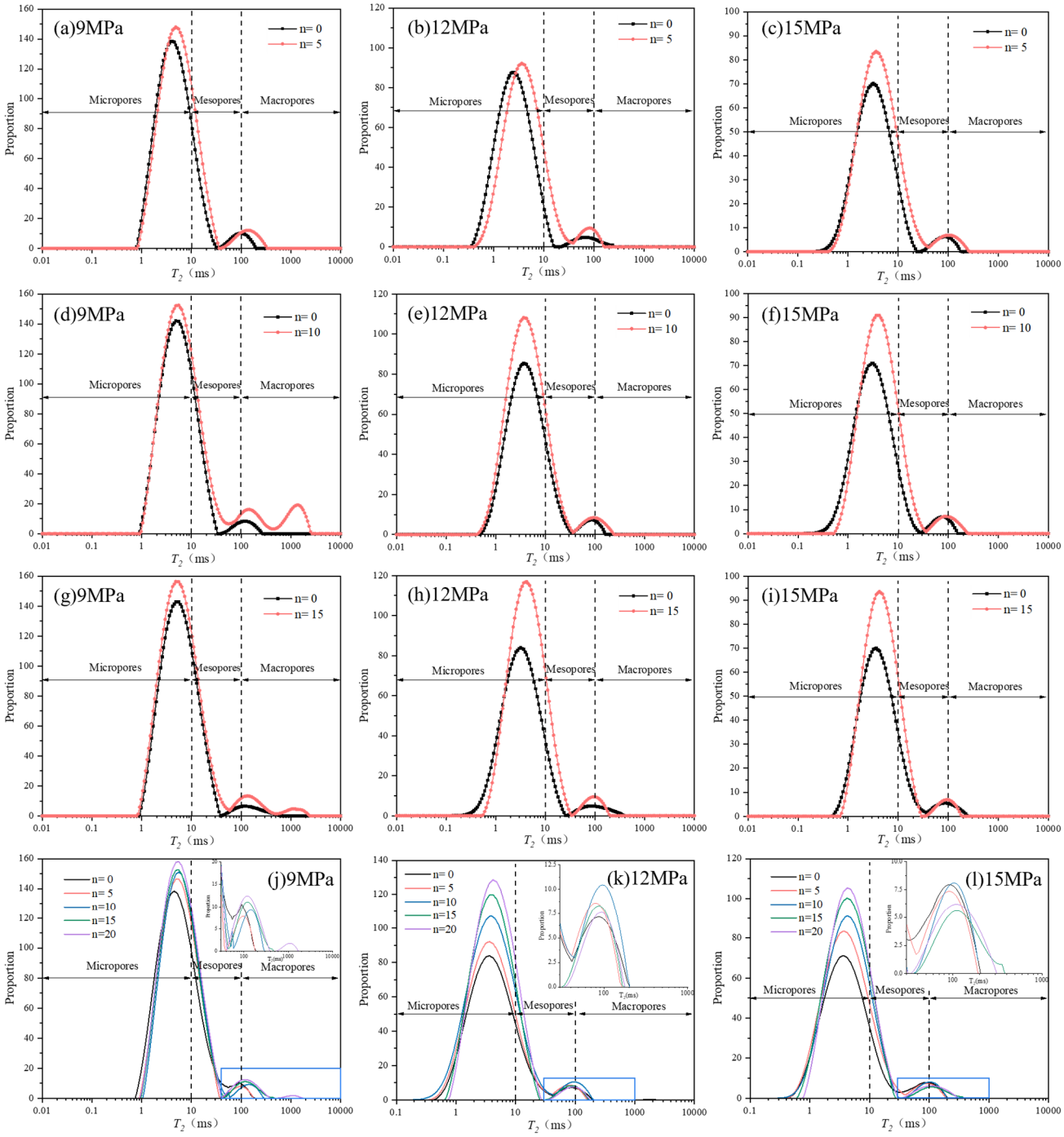

Figure 8. T_2 spectrum distribution of samples under different dry–wet cycles.

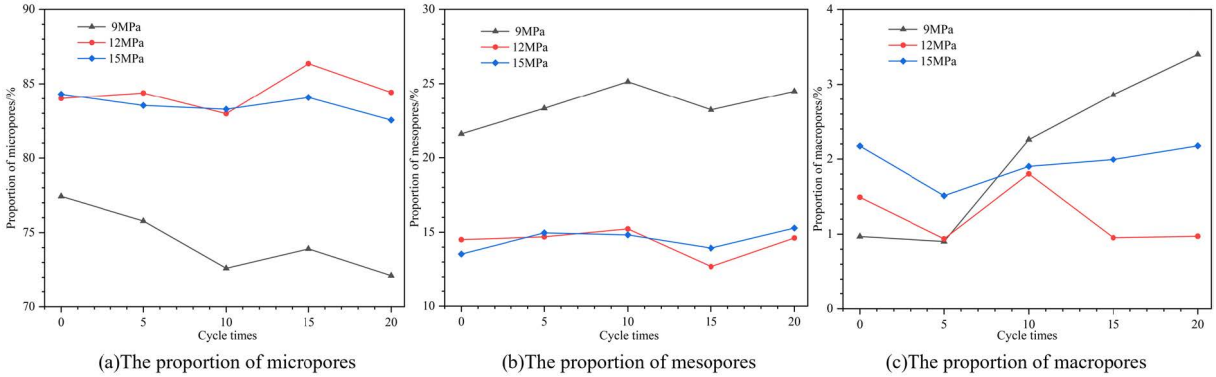

(a)The proportion of micropores (b)The proportion of mesopores (c)The proportion of macropores

Figure 9. Variation curves of different pore proportions with dry–wet cycles.

As can be seen from Figure 8, within the range of confining pressure and unloading amount of the test, the pore range of samples spans three kinds of pores, and the T_2 spectrum of the rock basically shows two peaks; only the T_2 spectrum of some samples with initial confining pressure of 9 MPa shows three peaks. Figure 8j,k,l show the damage caused by water–rock interaction gradually accumulates with the increase of dry–wet cycles, and the initial unloading damage is superimposed, resulting in the third peak in the T_2 spectrum of some rocks, and the peak value of the first peak of all rocks is much larger than other peaks. It can be seen that the pore size distribution inside the rock is uneven. The number of pores within the range of the first peak accounts for the vast majority of the total pores of the rock—that is, most of the pores in the rock are micropores.

As can be seen from Figure 9, with the increase of cycles, the proportion of micropores in the sample with initial confining pressure of 9 MPa decreases obviously, while the proportion of mesopores and macropores increases. For the samples with initial confining pressure of 12 MPa and 15 MPa, the proportion of mesopores and macropores increases significantly when the proportion of micropores decreases during the dry–wet cycle. Combined with the T_2 spectrum distribution of samples in Figure 8, it can be seen that the total pore volume of each unloaded sample increased with the increase of cycles, and the damage degree of samples gradually accumulated.

By comparing Figure 8, it can be seen that the overall pore of unloaded samples increases further after the dry–wet cycle, and the sample continues to deteriorate. When the dry–wet cycle is 5, the T_2 spectrum overall increased and shifted to the right, the first peak value increased slightly, and the third peak appeared in some samples, indicating that cracks with larger diameter were generated. When the dry–wet cycles were 10 and 15, the T_2 spectrum continued to shift to the right and the first peak value increased more obviously, and the corresponding peak value changed more obviously with cycles.

From a comprehensive comparison of Figure 8j,k,l, it can be concluded that unloaded samples with the initial confining pressure of 9 MPa are most significantly affected by the dry–wet cycle. In the range of 5 cycles and 15 cycles, the main pore type of samples, namely the first peak value, increases more evenly. It can be seen that the number and diameter of the pores in the sample increase uniformly as a whole—that is, they are in the stage of stable development of cracks. The T_2 spectrum of 20 dry–wet cycles basically includes all the T_2 spectrum after the previous cycles, and the first peak value and the pore range increases, which shows a large expansion of pores. The results show that the specimen has been affected by the hydrological effect to a large extent after 20 dry–wet cycles. The T_2 spectrum reflects the phenomenon that the pore structure of the sample increases and the structural compactness decreases with the increase of dry–wet cycles.

The analysis shows that the pore volume of unloaded samples increases with wet-dry cycles increasing. The peak shifts to the right and the pore diameter are larger, which is the result of the development of the inner part of the microcracks towards the increase of the cracks. It can be seen that the unloading effect of samples will cause the smaller pores to develop into larger pores and the new cracks to develop into small pores. With the increase

of cycles, the confining pressure unloading effect on the sample is more significant, the water–rock interaction is stronger, and the deterioration degree of the sample is higher.

4.2. T_2 Spectrum Area

The change of the integral area of T_2 spectrum distribution reflects the change of pore volume of the sample after different dry–wet cycles. The spectral area of each peak of the sample after different dry–wet cycles is shown in Table 3. The variation curves of the average spectral area of the sample with dry–wet cycles is shown in Figure 10, where the cycle is 0, which represents the state after unloading.

Table 3. Table of the average NMR spectrum area of samples under different dry–wet cycles.

Number of Cycles	Initial Confining Pressure	Confining Pressure of Unloading	Total Spectrum Area	The First Peak Area	The First Peak Proportion	The Second Peak Area	The Second Peak Proportion	The Third Peak Area	The Third Peak Proportion
0	9	5.4	4389.35	4194.54	95.58%	194.80	4.42%		
5			4539.15	4411.48	97.19%	127.67	2.81%		
10			4905.95	4544.73	92.91%	219.03	4.37%	142.19	2.72%
15			5004.06	4705.57	94.05%	263.10	5.27%	35.39	0.68%
20			5454.88	5197.32	95.28%	240.79	4.41%	16.77	0.31%
0	12	6.4	2701.28	2590.86	95.92%	110.42	4.08%		
5			2971.24	2847.40	95.83%	123.84	4.17%		
10			3565.12	3411.49	95.69%	153.63	4.31%		
15			3621.99	3491.41	96.40%	130.57	3.60%		
20			3788.88	3683.43	97.22%	105.45	2.78%		
0	15	8.0	2231.34	2119.74	95.00%	111.60	5.00%		
5			2721.35	2600.96	95.58%	120.39	4.42%		
10			2854.54	2730.00	95.64%	124.54	4.36%		
15			2925.39	2824.83	96.55%	100.56	3.45%		
20			3108.30	2984.03	96.00%	124.27	4.00%		

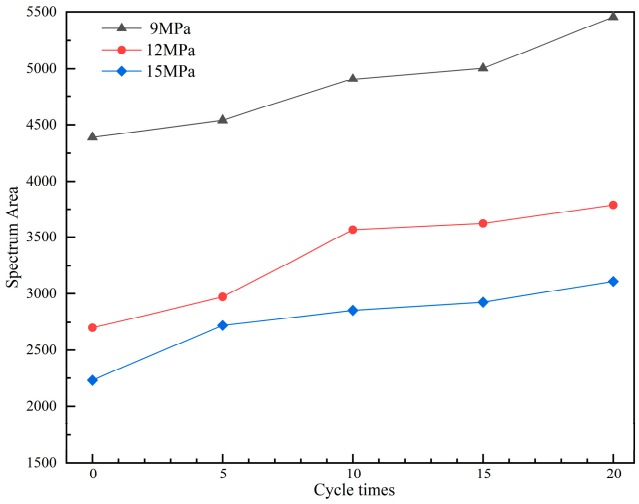

Figure 10. Variation curves of the total spectrum area with dry–wet cycles.

The NMR information and pore distribution of unloaded samples under different confining pressures are basically the same, and the distribution of the spectrum area of each sample is also very similar. Combined with the data in Table 3, it can be seen that the distribution of pore structures in the sample is uneven; the micropores account for the vast majority of all pore types and exceed 90%. When the dry–wet cycle is 0 (after unloading and before the dry–wet cycle), the total peak area of the sample is quite different. It can be seen that different initial confining pressures have a great influence on the internal pore structure of the sample. Under the same unloading amount, as the initial confining pressure increases, the total area of the spectrum decreases from 4389.35 to 2231.34, and the reduction ratio reaches 49.16%.

It can be seen from Figure 10 and Table 3 that under the same confining pressure and unloading amount, the total spectrum area of unloaded samples increases with the dry–wet

cycle, and the pore volume of samples increases. The maximum increase ratio of the total area of the spectrum is 21.96% when the dry–wet cycle is 0–5, the maximum is 19.98% when the cycle is 5–10, and it is only 2.49% when the cycle is 10–15. It can be seen that in the early stage of dry–wet cycles, the internal structure of unloaded samples was significantly affected by dry–wet cycles. In a certain range, the change trend of spectrum area tends to be gentle—that is, the internal structure of the sample is gradually accumulated by the dry–wet cycle, but the influence sensitivity is reduced. During 15–20 cycles, the maximum increase of total spectrum area is 9.00%, which is larger than that during 10–15 cycles. It shows that during this period, the porosity of the sample increased significantly, and the influence of the dry–wet cycle was close to the structural damage limit of unloaded samples.

In summary, the damage of the dry–wet cycle to unloaded samples is a cumulative process. On the one hand, the damage cracks caused by the early unloading provide more crack channels for the dry–wet cycle. Water easily infiltrates along crack channels, and the pore water pressure increases, thus forming inter-layer expansion and inter-particle expansion and increasing the cracks. At the same time, water molecules slowly penetrate into the sample along the cracks, causing the dissolution of soluble minerals and cements and also causing the closed pores formed by the cements to gradually transform into open pores. The micropores continue to expand and penetrate, the number of pores gradually increases, and the pore size and the volume increases.

5. Discussion

Wave velocity tests and NMR analysis can be used to evaluate the internal structure of unloaded rocks. Based on the above tests, the pore structure evolution of unloaded samples under dry–wet cycle was analyzed in detail through the mass, P-wave velocity, and NMR results. With the strengthening of dry–wet cycles, the P-wave velocity of the sample decreases continuously, indicating that the pore structure showed a gradual deterioration trend. The change of mass shows a three-stage change trend of rapid decline, uniform decline, and stability. T_2 spectrum distribution and spectrum area data show that the pore diameter increases with the increased cycling. It can be seen that the overall pore diameter and volume continue to increase with the strengthening of dry–wet cycles.

This article involves multiple analysis angles such as mass, wave speed, and pores and realizes macro and micro-angle and multi-parameter change analysis of the same sample, thereby showing the evolution and damage of the pore structure of the sample with the dry–wet cycle from different angles. As the dry–wet cycle continues, various dissolved substances in the sample are transported, causing mass loss. As the cycles increase, the content of soluble substances inside the sample continues to decrease, which manifests as a gradual decrease and tends to be stable in the percentage of mass reduction in the middle and late stages of the cycle. The growth rate of the sample pore size and number gradually decreases, which is manifested in the gradual decrease of the wave speed reduction percentage, and the T_2 spectrum distribution and spectral area growth amplitude decreases.

In summary, it can be seen from the above analysis that the dry–wet cycle affects the crack development time, thereby causing differential deterioration of the physical and mechanical properties of the sample. Combining the aforementioned quantitative reflections of mass, wave velocity, and NMR parameters on the pore structure and their evolution with cycles, the mechanism of the dry–wet cycle on unloaded samples can be divided into three periods: the early stage, the middle stage, and the late stage. The schematic diagram of the deterioration mechanism of the sample under the dry–wet cycle is drawn, as shown in Figure 11. Taking the longitudinal direction of the model as the analysis angle, the upper and lower ends of the model are the surface layer, and the middle of the model is the deep layer. The blue filling represents water molecules, the yellow filling represents cement, and the gray inclusions represent mineral particles.

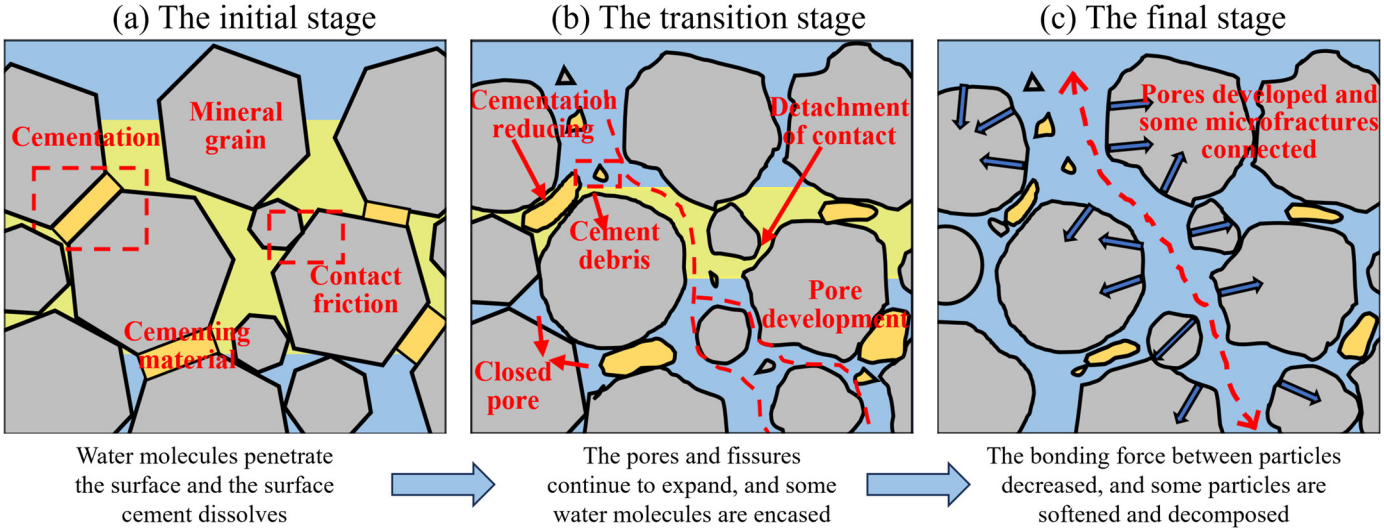

Figure 11. Microscopic deterioration model of unloaded samples at each stage under dry–wet cycles.

In the initial stage of the dry–wet cycle, due to the low interaction intensity, water molecules infiltrate into the surface layer along the pores and cracks of the sample, and the surface layer of the sample changes rapidly. Various types of unstable cements on the surface dissolved when exposed to water, and the cementation effect decreased, resulting in microscopic changes. Cracks and pores gradually develop, providing more reaction contact surfaces for the next stage of the dry–wet cycle. During the structural evolution process, part of the deep water is adsorbed on the surface of the particles, and part of the water is wrapped in closed pores, which is the main reason for the smaller difference in mass reduction at this stage compared with the middle stage.

In the transition stage of the dry–wet cycle, the cumulative intensity is strengthened, and the crack development time gradually accumulates. On the one hand, the cement continues to dissolve, while on the other hand, on the basis of the development of surface pores and cracks in the early stage and the process of repeated dry–wet cycles, some cracks are generated at the contact of rock particles, closed pores are converted into open pores, and then water can enter deeper areas inside the rock, thus prompting the pores to continue to develop and expand from the surface to the inside.

In the final stage of the dry–wet cycle, the effect strength is further accumulated and strengthened, and the micro-morphology and structure of the sample undergo significant changes. A large number of microcracks and pores are gradually collected on the basis of medium-term expansion, and secondary cracks are derived, causing the development, expansion, and even penetration of secondary cracks, thus causing the penetration of pores and cracks in large quantities. During this process, water is no longer wrapped, the adsorption force decreases, the fluidity increases, and water molecules flow in and out in large quantities, causing the internal mineral particles to soften and decompose, resulting in a significant reduction in the density of the sample structure and a gradual loosening of the microstructure, which is manifested as significant deterioration in mechanical properties.

6. Conclusions

Based on the consideration of the field environment, dry–wet cycles and NMR tests were carried out on unloaded samples. Combined with wave velocity and NMR results, the micro-pore structure evolution law of unloaded sandstone after different dry–wet cycles was studied. The main conclusions are as follows:

(1) As the dry–wet cycles increase, P-wave velocity and mass change trends both reflect the progressive deterioration process of unloaded samples. Both P-wave velocity and mass show a three-stage change trend of “rapid decrease-slow decrease-stability”. As

the dry–wet cycle gradually intensifies, the pores of the sample continue to increase and the cumulative damage increases.

(2) Analysis of T_2 spectrum distribution and spectrum area shows that the smaller the initial confining pressure, the more significant the confining pressure unloading effect on samples, and the higher the degree of deterioration of the sample. As the cycles increase, the damage accumulation of unloaded samples intensifies, and the overall pore diameter and number further increase. The overall trend is that smaller pores evolve towards larger pores, accompanied by the generation of new cracks.

(3) The effects of unloading and dry–wet cycles cause changes in the microstructure of the specimen, resulting in significant degradation of the mechanical properties. The unloading effect causes the initial pores of the sample to increase, providing channels for the dry–wet cycle. During the dry–wet cycle, the soluble cements existing between the particles inside the sample gradually dissolve and connect, which weakens the cohesion and friction between the particles inside the sample, resulting in a gradual reduction in the internal skeleton constraints of the sample; the particle structure becomes loose, and the original microcracks continue to develop and expand.

Author Contributions: Data curation, L.C. and Z.L.; Investigation, S.G. and Z.S.; Methodology, X.C., L.C., S.G., Z.L. and Z.S.; Writing—original draft, L.C.; Writing—review and editing, L.C. and X.C. All authors have read and agreed to the published version of the manuscript.

Funding: This study was supported by the National Natural Science Foundation of China (Grant No. 51979218, U1965107).

Data Availability Statement: The data used to support the findings of this study are available from the corresponding author upon request.

Acknowledgments: We would like to thank Xi'an University of Science and Technology for providing the test equipment.

Conflicts of Interest: The authors declare no competing interests.

References

1. Rinaldi, M.; Casagli, N. Stability of streambanks formed in partially saturated soils and effects of negative pore water pressures: The sieve river (Italy). *Geomorphology* **1999**, *26*, 253–277. [CrossRef]
2. Li, J.L. *Unloading Rock Mass Mechanics*; China Water and Power Press: Beijing, China, 2003.
3. Qiu, S.L.; Feng, X.T.; Xiao, J.Q.; Zhang, C.Q. An Experimental Study on the Pre-Peak Unloading Damage Evolution of Marble. *Rock Mech. Rock Eng.* **2014**, *47*, 401–419. [CrossRef]
4. Panaghi, K.; Takemura, T.; Asahina, D.; Takahashi, M. Effects of stress path on brittle failure of sandstone: Difference in crack growth between tri-axial compression and extension conditions. *Tectonophysics* **2021**, *810*, 228865. [CrossRef]
5. Walton, G.; Gaines, S.; Alejano, L.R. Validity of continuous-failure-state unloading triaxial tests as a means to estimate the residual strength of rocks. *J. Rock Mech. Geotech. Eng.* **2021**, *13*, 717–726. [CrossRef]
6. Abierdi, Y.X.; Zhong, H.; Gu, X.; Liu, H.L.; Zhang, W.G. Laboratory Model Tests and DEM Simulations of Unloading-Induced Tunnel Failure Mechanism. *CMC-Comput. Mater. Con.* **2020**, *63*, 825–844. [CrossRef]
7. Huang, D.; Li, Y.R. Conversion of strain energy in Triaxial Unloading Tests on Marble. *Int. J. Rock Mech. Min.* **2014**, *66*, 160–168. [CrossRef]
8. Walton, G.; Gaines, S. Evaluation of stress path and load rate effects on rock strength using compression testing data for Stanstead Granite. *Int. J. Rock Mech. Min.* **2023**, *169*, 105455. [CrossRef]
9. Wang, R.B.; Xu, B.; Wan, Y.; Wang, H.; Wang, W.; Meng, Q. Characteristics of unloading damage and permeability evolution of sandstone under hydro-mechanical coupling. *Eur. J. Environ. Civ. Eng.* **2020**, *27*, 2566–2575. [CrossRef]
10. Sheng, M.Q.; Mabi, A.; Lu, X.G. Study on Permeability of Deep-Buried Sandstone under Triaxial Cyclic Loads. *Adv. Civ. Eng.* **2021**, *2021*, 6635245. [CrossRef]
11. Wang, Y.; Feng, W.K.; Hu, R.L.; Li, C.H. Fracture Evolution and Energy Characteristics During Marble Failure Under Triaxial Fatigue Cyclic and Confining Pressure Unloading (FC-CPU) Conditions. *Rock Mech. Rock Eng.* **2020**, *54*, 799–818. [CrossRef]
12. Li, D.Y.; Sun, Z.; Xie, T.; Li, X.; Ranjith, P. Energy evolution characteristics of hard rock during triaxial failure with different loading and unloading paths. *Eng. Geol.* **2017**, *228*, 270–281. [CrossRef]
13. Abi, E.; Yuan, H.C.; Cong, Y.; Wang, Z.; Jiang, M. Experimental Study on the Entropy Change Failure Precursors of Marble under Different Stress Paths. *KSCE J. Civ. Eng.* **2023**, *27*, 356–370. [CrossRef]

14. Zhang, H.X.; Lu, K.P.; Zhang, W.Z.; Li, D.; Yang, G. Quantification and acoustic emission characteristics of sandstone damage evolution under dry-wet cycles. *J. Build. Eng.* **2022**, *48*, 103996. [CrossRef]
15. Guo, P.Y.; Gu, J.; Su, Y.; Wang, J.; Ding, Z. Effect of cyclic wetting-drying on tensile mechanical behavior and microstructure of clay-bearing sandstone. *Int. J. Coal Sci. Technol.* **2021**, *8*, 956–968. [CrossRef]
16. Wang, Z.J.; Liu, X.R.; Fu, Y.; Liang, Z.; Wen, Y. Erosion analysis of argillaceous sandstone under dry-wet cycle in two pH conditions. *Rock Soil Mech.* **2016**, *37*, 3231–3239. [CrossRef]
17. Chen, X.X.; He, P.; Qin, Z. Damage to the Microstructure and Strength of Altered Granite under Wet-Dry Cycles. *Symmetry* **2018**, *10*, 716. [CrossRef]
18. Qin, Z.; Fu, H.L.; Chen, X.X. A study on altered granite meso-damage mechanisms due to water invasion-water loss cycles. *Environ. Earth Sci.* **2019**, *78*, 428. [CrossRef]
19. Ma, J.W.; Niu, X.X.; Xiong, C.R.; Lu, S.; Xia, D.; Zhang, B.; Tang, H. Experimental Investigation of the Physical Properties and Microstructure of Slate under Wetting and Drying Cycles Using Micro-CT and Ultrasonic Wave Velocity Tests. *Sensors* **2020**, *20*, 4853. [CrossRef]
20. An, R.; Kong, L.W.; Zhang, X.W.; Li, C. Effects of dry-wet cycles on three-dimensional pore structure and permeability characteristics of granite residual soil using X-ray micro computed tomography. *J. Rock Mech. Geotech. Eng.* **2022**, *14*, 851–860. [CrossRef]
21. Fang, J.C.; Deng, H.F.; Li, J.L.; Assefa, E. Study on the seepage characteristics and degradation mechanism of a single-jointed sandstone under the cyclic dry-wet process in the Three Gorges reservoir. *Bull. Eng. Geol. Environ.* **2021**, *80*, 8123–8136. [CrossRef]
22. Dang, C.; Sui, Z.L.; Yang, X.Y.; Ge, Z. Pore Changes in Purple Mudstone Based on the Analysis of Dry-Wet Cycles Using Nuclear Magnetic Resonance. *Shock Vib.* **2022**, *2022*, 5578401. [CrossRef]
23. Fu, Y.; Wang, Z.J.; Liu, X.R.; Wen, Y.; Miao, L.-L.; Liu, J.; Dun, Z.-Y. Meso damage evolution characteristics and macro degradation of sandstone under wetting-drying cycles. *Chin. J. Geotech. Eng.* **2017**, *39*, 1653–1661. [CrossRef]
24. Liu, X.R.; Jin, M.; Li, D.; Zhang, L. Strength deterioration of a Shaly sandstone under dry–wet cycles: A case study from the Three Gorges Reservoir in China. *Bull. Eng. Geol. Environ.* **2018**, *77*, 1607–1621. [CrossRef]
25. Wen, Y.; Liu, X.R.; Fu, Y. Study on Deterioration of Strength Parameters of Sandstone Under the Action of Dry-Wet Cycles in Acid and Alkaline Environment. *Arab. J. Sci. Eng.* **2018**, *43*, 335–348.
26. Huang, X.; Pang, J.Y.; Liu, G.C.; Chen, Y. Experimental Study on Physicomechanical Properties of Deep Sandstone by Coupling of Dry-Wet Cycles and Acidic Environment. *Adv. Civ. Eng.* **2020**, *2020*, 2760952. [CrossRef]
27. Wang, L.L.; Bornert, M.; Héripré, E.; Yang, D.; Chanchole, S. Irreversible deformation and damage in argillaceous rocks induced by wetting/drying. *J. Appl. Geophys.* **2014**, *107*, 108–118. [CrossRef]
28. Yang, X.J.; Wang, J.M.; Zhu, C.; He, M.; Gao, Y. Effect of wetting and drying cycles on microstructure of rock based on SEM. *Environ. Earth Sci.* **2019**, *78*, 183. [CrossRef]
29. Ma, D.H.; Yao, H.Y.; Xiong, J.; Zhu, D.; Lu, J. Experimental Study on the Deterioration Mechanism of Sandstone under the Condition of Wet-Dry Cycles. *KSCE J. Civ. Eng.* **2022**, *26*, 2685–2694. [CrossRef]
30. Zhao, B.Y.; Li, Y.F.; Huang, W.; Yang, J.; Sun, J.; Li, W.; Zhang, L.; Zhang, L. Mechanical characteristics of red sandstone under cyclic wetting and drying. *Environ. Earth Sci.* **2021**, *80*, 738. [CrossRef]
31. Deng, H.F.; Zhang, H.B.; Li, J.L.; Wang, C.; Zhang, Y.; Wang, W.; Hu, Y. Effect of water-rock interaction on unloading mechanical properties and microstructure of sandstone. *Rock Soil Mech.* **2018**, *39*, 9. [CrossRef]
32. *GB/T 50266-2013*; Standard for Test Methods of Engineering Rock Mass. China Planning Press: Beijing, China, 2013.
33. Chen, X.Z.; Chen, L.L.; Ma, B.; Zhang, X.; Du, W.; Wang, X.; Yang, C. Mechanical-characteristic evaluation of excavation unloading rock mass subject to high-temperature conditions. *Eng. Fail. Anal.* **2021**, *130*, 105757. [CrossRef]
34. Fu, Y. *Study on Water-Rock Interaction with the Cyclic Drying-Wetting Effect on Rock*; Chongqing University: Chongqing, China, 2010.
35. Liang, N.H.; Liu, X.R.; Bao, T.; Wei, Q.P. Experimental Study on the Characteristic of Seepage with Unloading Rock Mass. *J. Chongqing Univ. Nat. Sci. Ed.* **2005**, *28*, 136–138.
36. Grove, J.R.; Croke, J.; Thompson, C. Quantifying different riverbank erosion processes during an extreme flood event. *Earth Surf. Process. Landf.* **2013**, *38*, 1393–1406. [CrossRef]
37. Jin, P.H.; Hu, Y.Q.; Shao, J.X.; Liu, Z.; Feng, G.; Song, S. Influence of temperature on the structure of pore-fracture of sandstone. *Rock Mech. Rock Eng.* **2020**, *53*, 1–12. [CrossRef]